RSC Advances

ROYAL SOCIETY OF CHEMISTRY

www.rsc.org/advances

The dependence of the non-linear creep properties for TATB-based polymer bonded explosives on the molecular structure of polymer binder

Congmei Lin, Shijun Liu, Zhong Huang, Guansong He, Feiyan Gong, Yonggang Liu, Jiahui Liu *

The influences of molecular structure of polymer binders on the mechanical properties and non-linear time dependent creep of the 1,3,5-triamino-2,4,6-trinitrobenzene (TATB)-based polymer bonded explosives (PBXs) at different temperatures and stresses were investigated. A copolymer of chlorotrifluoroethylene and vinylidene fluoride (PF1) and a copolymer of chlorotrifluoroethylene, vinylidene fluoride, tetrafluoroethylene, and hexafluoropropylene (PF2) were used as polymer binders. An increase of the storage modulus and glass transition temperature was observed for PF2, compared to that of PF1. The compressive and tensile properties of TATB-based PBX with PF2 were higher than the one with PF1 at both ambient temperature and elevated temperature. The creep resistance also showed clear dependence on the molecular structure of polymer binders. It was found that the incorporation of tetrafluoroethylene and hexafluoropropylene comonomers in PF2 resulted in a decrease of the constant creep strain rate and the maximal creep strain values and an increase of creep rupture time for TATB-based PBX. Non-linearity in the creep response was modeled using the six-element mechanical model. The predicted theoretical results coincided quite well with the experimental data. Compared with the formulation containing PF1 as binder, an increase in the elastic modulus E_2, E_3 and bulk viscosity η_4 was observed for TATB-based PBX with PF2 under the same conditions. Three-point bending master curves of creep strain were constructed using a time-temperature superposition (TTS) concept. The formulation with PF2 had shown consistently lower creep strain than the formulation with PF1 in the entire time scale.

Key words: applied chemistry TATB polymer bonded explosive molecular structure non-linear creep properties

1. Introduction

During the past decades, as a kind of particle highly filled composite material, polymer bonded explosive (PBX) is extensively applied in military field ranging from rocket propellants to the explosive charge.[1,2] During the long-term storage and transport, the PBX is subjected to combined thermal and mechanical loads, and the creep relaxation behavior takes place. In recent years, the creep behavior of polymer-based composites is of great interest in the academic and industrial fields because of its significant influences on the dimensional stability, long-term durability and reliability. The addition of various inorganic fillers into the polymer matrix is a common and convenient method to improve creep resistant of polymer.[3-5] However, the filler content in these composites is very low, which is totally different from PBX with high content explosive particles. A number of investigations on the creep behavior of PBXs have also been performed.[6,7] It is believed that the creep behavior of PBX is dependent on the type of explosive, the percentage and type of binder, the stress level and test temperature. A custom designed apparatus which uses a

Institute of Chemical Materials, China Academy of Engineering Physics, Mianyang, Sichuan 621900, P. R. China.
E-mail: huiihuii@163.com; Fax: +86-816-2495856; Tel: +86-816-2482005.

combination of extensometers and linear variable differential transformers coupled with a data acquisition system, thermal controls, and gravitational loading has been established to measure the time-dependent creep strain in the plastic-bonded explosives with high fidelity.[8] Micro-analysis of the creep properties of PBX simulation has been performed using SEM combined with the digital image correlation (DIC) method.[9] During the process of high temperature creep, extensive cracks are first formed followed by the initiation and extension of shear cracks, eventually joining and causing a macroscopic fracture within the material. The main microscopic fracture mode has been found to be intercrystalline cracking and binder tearing failure.

It is now well accepted that as one kind of the most commonly used binders with the advantages of good physical and chemical stability, excellent aging resistance and heat resistance, and great conpatibility with other components in composite explosives, fluoropolymer is of great interest in the academic and industrial fields.[10-14] Compared to general hydrocatbons, the high density of fluoropolymer brings on the enhancement of the density and performance for PBX. Furthermore, the oxygen balance is enhanced with the hydrogen atom (fuel) on the polymer main chain replaced by fluorin atom (oxidizer), resulting in a better properties of composite explosives. Consequently, several PBX materials have been formulated with fluoropolymer as a binder in the last decades, such as LX-17 (92.5% 1,3,5-triamino-2,4,6-trinitrobenzene TATB and 7.5% a copolymer of chlorotrifluoroethylene and vinylidene fluoride kel-F800 by weight) and PBX-9502 (95% TATB and 5% kel-F800 by weight).[15-17]

Generally, PBX is comprised of 90-95% weight of explosive crystals and 5-10% weight of a polymeric binder.[18] The polymeric matrix in PBX is a typical viscoelastic material, and the creep deformation is inevitable at a certain temperature and loading stress.[19-23] It is recognized that despite the polymer content being very low, the creep property of the polymer is the main factor in influencing the creep damage properties of PBX.[24]

However, researches on the influences of molecular structure of the polymer binder on the creep performance of PBX are relatively limited. In our previous wok, the studies on the effects of the addition of reinforcing agent (styrene copolymer) to the original fluoropolymer binder system on the three-point bending creep behaviors have been conducted.[25] The experimental results show that owing to the addition of styrene copolymer with high glass transition temperature and high mechanical strength, the creep resistance performance of the modified formulation is improved with reduced creep strain and constant creep rate and prolonged creep failure time.

The fundamental understanding of the effects of molecular structure of polymer binder on the creep relaxation of PBX is still unclear. In this work, we focus on two kinds of fluoropolymer with different molecular structure served as the binder. The main objective of this study is to investigate the creep processes of TATB-based PBX by three-point bending creep measurements. The studies on the effects of molecular structure on the dynamic mechanical behaviors and static mechanical properties of PBXs are also conducted.

2. Experimental Section

2.1 Materials

TATB (purity 99 %, particle size about 17 μm) was obtained from Institute of Chemical Materials, CAEP, China. Two fluoropolymers with different molecular structure were used as polymer binder, i.e. a copolymer of chlorotrifluoroethylene and vinylidene fluoride, labeled as PF1 and a copolymer of chlorotrifluoroethylene, vinylidene fluoride, tetrafluoroethylene, and

hexafluoropropylene, labeled as PF2. The molecular structures of PF1 and PF2 were -[-(CF_2-CH_2-)$_a$-(-CF_2-CFCl-)$_b$-]$_n$- and -[(-CF_2-CH_2-)$_a$-(-CF_2-CFCl-)$_b$-(-CF_2-CF_2-)$_c$-(-CF_2-$CFCF_3$-)$_d$)]$_n$-. The weight average molecular weight of PF1 is 1.13 $\times 10^5$ g/mol with a polydispersity index of 2.13. The weight average molecular weight of PF2 is 5.47×10^4 g/mol with a polydispersity index of 1.93. Both PF1 and PF2 were provided by Zhonghao Chenguang Chemical Industry Co., Ltd. China. The other chemicals and reagents used in the presented study were commercially purchased and used as received.

2.2 Sample preparation

A formulation which contained 95 % TATB and 5 % PF1 by weight was labeled as PBX-1. Another formulation with TATB and PF2 with the same molar ratio was prepared, labeled as PBX-2. Firstly, TATB (180 g) was added to H_2O (180 mL) and dispersed whilst stirring at 70 ℃ in a vacuum. Then the polymer binder solution with ethyl acetate and butyl acetate as the mixed solvent was added dropwise. After removing the organic solvent, the precipitate was filtered, washed to give the molding powders of TATB-based formulations. Before mould pressing, the molding powders were carefully dried in a vacuum oven at 60 ℃ for 12 h to eliminate the influences of moisture content on the experimental results. Afterwards, the molding powder product was pressed in a mould and transformed into explosive pellet. The pellet density was about 97% of the theoretical density after compression.

2.3 Mechanical characterization of the composites

All static mechanical tests were performed with a universal testing machine (5582, INSTRAN, USA). According to GB/T1040-2006, the dumbbell-shaped specimens of fluoropolymers were punch-cut from the compression-molded sheets and tested in a uniaxial tensile configuration under a constant crosshead speed of 50 mm/min. The specimens of explosive pellet with dimensions of ϕ 20 mm × 20 mm and ϕ 20 mm × 6 mm (diameter × height) for compressive (according to GJB-772A-97 standard method 418.1)[26] and Brazilian test were molded at 120 ℃. The details of the Brazilian test process were reported by Wen et al.[27] At least three specimens of each composite were tested, and the average values were reported.

Dynamic mechanical analysis (DMA) of fluoropolymer and TATB-based formulations with dimensions of 30 mm × 10 mm × 1~2 mm (length × width × thickness) was conducted with a DMA 242C apparatus (Netzsch, Germany) in three-point bending creep mode at a frequency of 1 Hz. The heating rate was set for 1 ℃/min.

2.4 Three-point bending creep tests

The creep tests were recorded with a Netzsch DMA 242C instrument using a three-point bending sample holder with a span of 20 mm. Three-point bending creep tests were carried out on specimens 30 mm long × 10mm wide and approximately 1.5 mm thickness. The specimens were loaded for 5400 s at four temperatures and three stress levels.

3. Results and Discussion

3.1 The properties of polymer binders

Fig. 1 shows the influence of molecular structure on the DMA curves of polymer binders. It can

be seen that the incorporation of tetrafluoroethylene and hexafluoropropylene comonomers in PF-2 results in an increase of the storage modulus (E') in the whole temperature range, compared to that of PF-1. The storage modulus gradually decreases with the experimental temperature, then begins to abruptly decline, and finally keeps constant. The onset temperature of the storage modulus in the DMA curve, i.e. the temperature at which the storage modulus begins to abruptly decline for PF-2 is 50.1 ℃, which is 12.8 ℃ higher than that of PF-1 sample (37.3 ℃). At 60 ℃, the storage modulus retention of the PF-2 is 32.3% (determined by the ratio of the modulus value at 60 ℃ to the modulus value at room temperature), while PF-1 is less than 2.7%.

The loss tangent data (tanδ) presented in Fig. 1b confirms the temperature dependence of the storage modulus but provide a more exact indication of the glass transition temperatures. The PF-1 shows the glass transition in the range 35-90 ℃ with a glass transition temperature (T_g) of 49.5 ℃ which is the peak value of the loss factor curves. PF-2 showed the glass transition in the range 50-100 ℃ with a T_g of 68.5 ℃, which is 19 ℃ higher than that of PF-1. It is well accepted that the glass transition temperature is affected by the chain structure of polymer. The increase of glass transition temperature is believed to be attributed to the introduction of the tetrafluoroethylene and hexafluoropropylene comonomers into the copolymer PF2. Due to the symmetrical substitution on the quaternary carbon for polyvinylidene fluoride (PVDF), the barrier to internal rotation of polymer main chain is low with good chain flexibility. Consequently, the glass transition of PVDF is visible at about -30 ℃.[28] Compared with PVDF, the substituent groups are manifolded and the glass transition temperature of polychlorotrifluoroethylene (PCTFE) investigated by Khanna[29] is reported to be 75 ℃. The replacement of all hydrogen atoms along the carbon backbone by fluorine atoms with higher polarity for polytetrafluoroethylene (PTFE), has a marked influnce on the internal rotation of polymer main chain and intermolecular reaction. It is clearly revealed the glass transition temperature for PTFE is 130 ℃.[30] The replacement of one out of every four fluorine atoms along the carbon backbone of PTFE with a larger CF_3 unit prevents the glass transition, resulting in a higher glass transition temperature of 150 ℃ for completely amorphous poly(hexafluoropropylene) (PHFP).[31] Therefore, copolymerisation with tetrafluoroethylene and hexafluoropropylene shifts the glass transition process to higher temperature, which is clearly visible on the DMA result.

The tensile mechanical tests of two fluoropolymers have also been conducted. The characteristics of the polymer binders, including glass transition temperature T_g, tensile strength and elongation at break are listed in Table 1. Compared with the PF-1, the tensile strength of PF-2 is increased by 5.9 %.

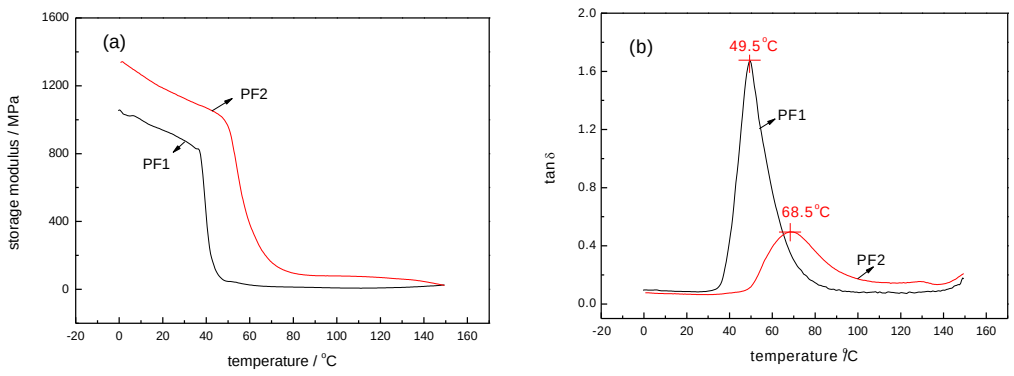

Fig. 1 Effects of molecular structure on the DMA curves of polymer binders: (a) storage modulus (E'), (b) loss

factor (tanδ).

Table 1 Property parameters of polymer binders.

sample	glass transition temperature / ℃	tensile strength / MPa	elongation at break / %
PF1	49.5	20.90	211.0
PF2	68.5	22.13	244.8

3.2 Characterization of the TATB-based PBXs

Fig. 2 indicates the dependence of the storage modulus (E') and loss factor (tanδ) on the temperature for pure TATB and TATB-based PBXs. Due to the small storage modulus for polymer binder (Fig. 1), the storage modulus of TATB-based PBX which contains 5% polymer binder is smaller than pure TATB. The excellent mechanical behavior and high glass transition temperature of the polymer binder PF-2 is reflected on the PBX-2, both on the magnitude and temperature dependence of storage modulus. PBX-2 shows higher storage modulus in the whole temperature range, compared to that of PBX-1. In addition, the storage modulus of PBX-1 strongly decreases with increasing temperature. While for PBX-2, the viscoelastic behavior is quite stable up to at least 120 ℃, with storage modulus decreasing slightly from 7.63 GPa at 0 ℃ to 5.93 GPa at 120 ℃. The storage modulus of PBX-2 at 60 ℃ (7.00 GPa) is at least 27.0% higher than that of PBX-1. There is no obvious transition process for pure TATB in the test temperature range, while the TATB-based PBX exists a glass transition temperature which is inflexion of the loss factor curves, corresponding to the T_g of corresponding polymer binder, as shown in Fig. 2b.

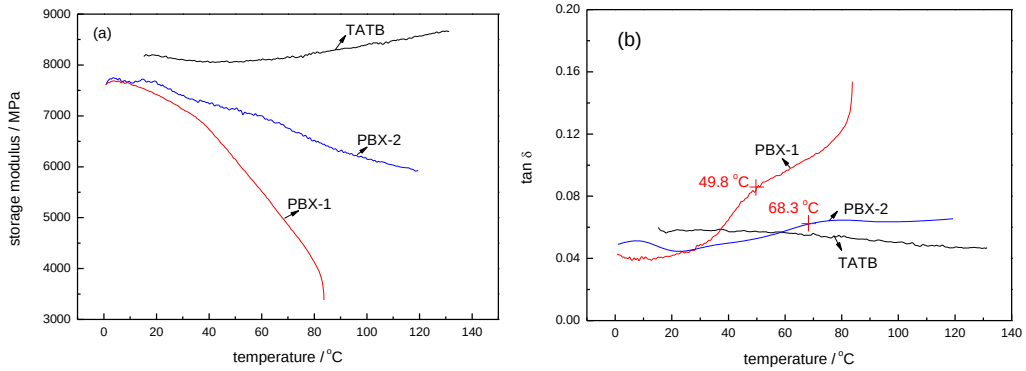

Fig. 2 Plot of storage modulus (E') and loss factor (tanδ) versus temperature for TATB-based PBXs: (a) storage modulus (E'), (b) loss factor (tanδ).

Brazilian test is initially used to estimate the properties of brittle materials such as rocks.[32,33] Then Brazilian test is introduced to the field of explosives by Johnson.[34,35] It is well accepted that the Brazilian disc test is the most convenient substitute of the direct tensile test in case of specimens made from brittle materials. The specimens of pure TATB and TATB-based PBXs have a shape of cylindrical pellets (20 mm ϕ by 6-20 mm height), and the compressive and Brazilian experiments are performed at room temperature and elevated temperature (60 ℃). The resulting relationship curve for stress and strain or displacement is shown in Fig. 3. Pure TATB and TATB-based PBXs fail in a brittle mode, as demonstrated by the sudden discontinuity in the stress-strain curve at the maximal stress. Compared with pure TATB, TATB-based PBXs show a significant increase in the mechanical strength and elongation at break under the same condition, indicating that the interfacial bonding role of polymer binder enhances the mechanical properties

of PBX. It can be observed that the higher the temperature, the smaller the compressive and tensile strength. As the temperature increases from 20 ℃ to 60 ℃, the compressive strength of PBX-1 decreases from 25.81 MPa to 15.46 MPa, declining by 40.1%, and the tensile strength of PBX-1 decreases from 4.76 MPa to 2.33 MPa, declining by 51.1%. This indicates that the temperature has a significant effect on the mechanical properties of TATB-based PBXs. PBX-1 displays a larger variation in mechanical properties than PBX-2 with increasing temperature. It can also be seen that PBX-2 have up to 7.2% and 4.2% higher compressive and tensile strength at 20 ℃ than PBX-1, and up to 33.9% and 17.2% higher compressive and tensile strength at 60 ℃ than PBX-1, which agrees with the above DMA results. These differences in mechanical properties are related to the differences in the glass transition temperature and mechanical response of the polymer binders within TATB-based PBXs.

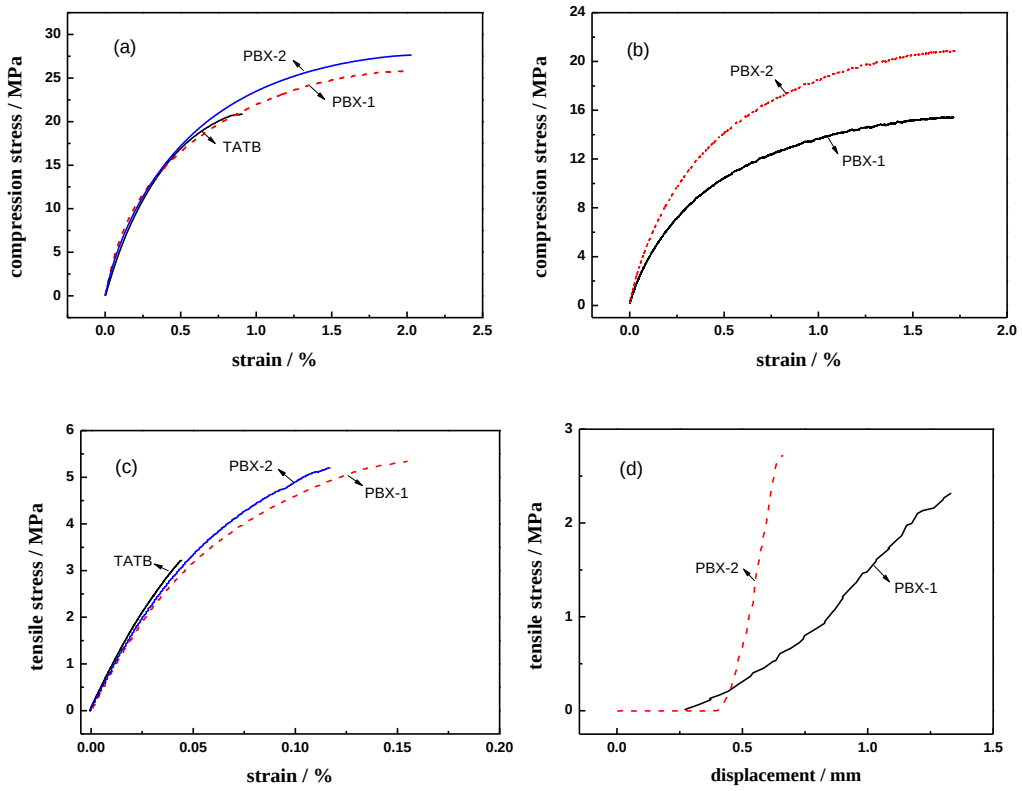

Fig. 3 The typical mechanical response for TATB-based PBXs at room temperature and elevated temperature: (a) compressive test at room temperature, (b) compressive test at 60 ℃, (c) Brazilian test at room temperature, (d) Brazilian test at 60 ℃.

3.3 Three-point bending creep tests

The creep tests are utilized to provide the time-dependent deformation under constant loads. Fig. 4 demonstrates the creep response for pure TATB and TATB-based PBXs samples as a function of time under different stresses at 60 ℃. Compared with pure TATB, TATB-based PBXs show a significant increase in the creep strain under the same condition. The results could be attributed to the viscoelastic properties of polymer binders. The instantaneous elastic deformation, high elastic deformation, and viscous flow are simultaneous during the creep process. Therefore, the creep strain of polymer binder is much bigger than pure TATB, leading to the increase of creep strain in

TATB-based PBXs with the addition of polymer binders.

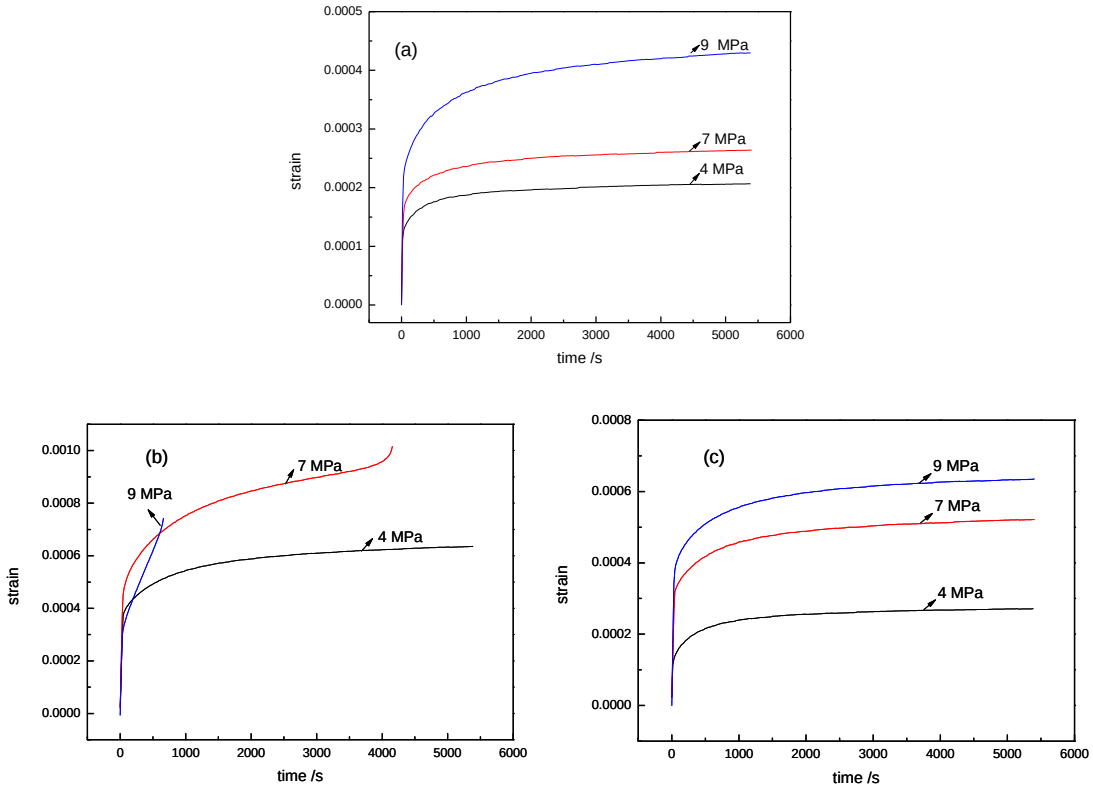

Fig. 4 Three-point bending creep strain curves of TATB-based PBXs under different stresses at 60 ℃: (a) pure TATB; (b) PBX-1; (c) PBX-2.

The constant creep strain rate is known to be a good indicator of the creep resistance of polymer composites. As an example, Fig. 5 presents the typical variation of the creep strain with the creep time for PBX-1 at 60 ℃/4 MPa. Usually, the creep strain varies linearly with the creep time during the steady state creep stage, as plotted in Fig. 5. The constant creep strain rate is the coefficient of creep strain to creep time which is acquired from the slope of the fitting line during the steady state creep stage.

Table 2 summarizes the creep performance parameters of TATB-based PBXs under different stresses at 60 ℃, including the constant creep strain rate, the maximal creep strain and creep rupture time. The experimental results demonstrates that the usage of PF2 with high glass transition temperature and high mechanical strength is an effective way to improve the creep properties of the formulations with reduced creep strain and constant creep strain rate and prolonged creep failure time. For example, it is found that the constant creep strain rate and the maximal creep strain of the PBX-1 at 60 ℃/4 MPa are 1.397×10^{-8} s^{-1} and 6.356×10^{-4}. With respect to the composite PBX-2 that contains 5% PF2, the constant creep strain rate and the maximal creep strain are reduced by 66.7% and 57.4%. Under higher loading stress (7 MPa and 9 MPa), the creep failure of the sample PBX-1 is occurred at 4155 s and 660 s, respectively. Under the same condition, the modified formulation displays a long-term creep process and no creep rupture time could be obtained, suggesting that the creep resistance is improved by the introduction of PF2. The constant creep strain rate, the maximal creep strain values, and creep failure time of the composites reflect the difference of the polymer binders: the replacement PF1 with PF2 binder is accompanied with a significant reduction in the constant creep strain rate and

the maximal creep strain and an increase of creep failure time.

Table 2. The creep performance parameters of TATB-based PBXs under different conditions.

sample	experimental conditions	constant creep strain rate / s^{-1}	maximal creep strain	creep rupture time / s
PBX-1	30 ℃/4 MPa	4.982×10^{-9}	2.300×10^{-4}	> 5400
	45 ℃/4 MPa	1.076×10^{-8}	3.899×10^{-4}	> 5400
	60 ℃/4 MPa	1.397×10^{-8}	6.356×10^{-4}	> 5400
	80 ℃/4 MPa	1.834×10^{-8}	8.246×10^{-4}	> 5400
	60 ℃/7 MPa	5.152×10^{-8}	1.020×10^{-3}	4155
	60 ℃/9 MPa	--	7.423×10^{-4}	660
PBX-2	30 ℃/4 MPa	3.294×10^{-9}	1.326×10^{-4}	> 5400
	45 ℃/4 MPa	3.341×10^{-9}	1.391×10^{-4}	> 5400
	60 ℃/4 MPa	4.654×10^{-9}	2.710×10^{-4}	> 5400
	80 ℃/4 MPa	5.973×10^{-9}	4.346×10^{-4}	> 5400
	60 ℃/7 MPa	9.631×10^{-9}	5.214×10^{-4}	> 5400
	60 ℃/9 MPa	1.111×10^{-8}	6.353×10^{-4}	> 5400

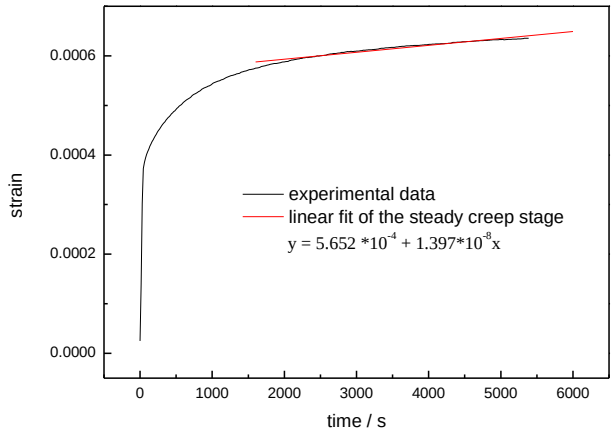

Fig. 5 The linear fit of the creep strain curves during steady creep stage of PBX-1 at 60 ℃/4 MPa.

A creep mechanism of PBX has been studied from the theory of deformation and sliding of molecular chain of the polymer by Ding et al.[24] It is shown that the creep property of the polymer is the main factor influencing on the creep-damage properties of the composite though polymer content is so little in amount. The motion of chain segment accounts for the enhanced three-point bending creep resistance of PBX-2. As mentioned above by DMA results, the glass transition temperatures of PF-1 and PF-2 are 49.5 ℃ and 68.5 ℃, respectively. The glass transition is dependent on the relative degree of freedom for molecular motion within a given polymeric material. The molecular features which either increase or reduce this mobility will cause differences in the value of T_g. The main molecular chain of PF1 composes of saturated single bond, therefore, molecular chain could internally rotate surrounding the single bond, leading to a low T_g. However, due to the fact that the main molecular chain of PF2 contains the comonomers of tetrafluoroethylene with high content of polarity fluorine atoms and hexafluoropropylene with high steric hindrance $-CF_3$ groups, the proportion of single bond which could internally rotate is small and chain stiffness is high, resulting in the hindrance of chain segment motion. During the

creep test at 60 ℃, the PF-1 is in the rubbery elastic state with freely chain segment movement. The PF-2 is in the glassy state with frozen chain segment. Consequently, the relaxation time of the motion of chain segment and intermolecular inner frictional resistance is higher for PF-2, which is beneficial to the creep resistance. Besides, the higher mechanical strength of PF-2 is another reason for the improved creep resistance of PBX-2.

The loading stress dependence of the creep response for the TATB-based PBXs in the range from 4 MPa to 9 MPa is also displayed in Fig. 4. As illustrated in Fig. 4, a prominent increase of the creep rupture time of TATB-based PBXs is achieved by the increase of loading stress. For example, the 60 ℃/7 MPa test resulted in the failure of PBX-1 at approximately 4155 s, while the sample did not show any signs of impending failure under lower stress (4 MPa) at the same temperature. When the loading stress is further increased to 9 MPa, the creep strain increases rapidly with creep time and final creep rupture occurs at 660 s. The decrease of viscosity which is caused by the increase of loading stress is believed to be the major contribution to this behavior. As a consequence, an easier motion of molecular chain is achieved as loading stress increases.

Fig. 6 describes the creep strain in relation to the temperature for pure TATB and TATB-based PBXs as a function of time under 4 MPa. As expected, compared with pure TATB, a prominent increase of the creep strain of TATB-based PBXs is achieved by the incorporation of polymer binder at all temperatures. The creep performance parameters of TATB-based PBXs at different temperatures are also listed in Table 2. As can be seen in Fig. 6 and Table 2, all of the specimens display a long-term creep process and no creep rupture time could be obtained within the observation time scale. Experiments show a significant increase in the creep strain and the constant creep strain rate of TATB-based PBXs with increased temperature. The maximal creep strain at 5400s and the constant creep strain rate of PBX-1 at 80 ℃ are measured to be 8.246×10^{-4} and 1.834×10^{-8} s^{-1}, respectively, which are 2.6-fold and 2.7-fold improvement in comparison to that at 30 ℃. A possible explanation is that this behavior could be related to the enhancement of thermodynamic mobility of the chains. The energy of thermodynamic motion and the intermolecular free space increase with increased temperature.

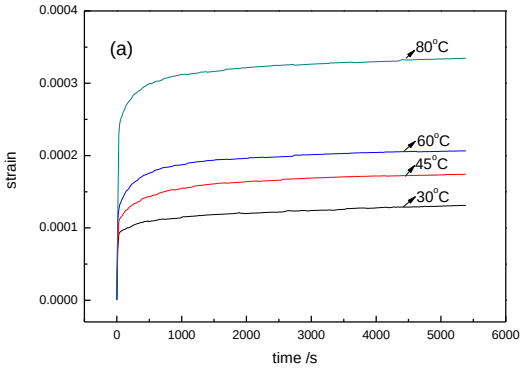

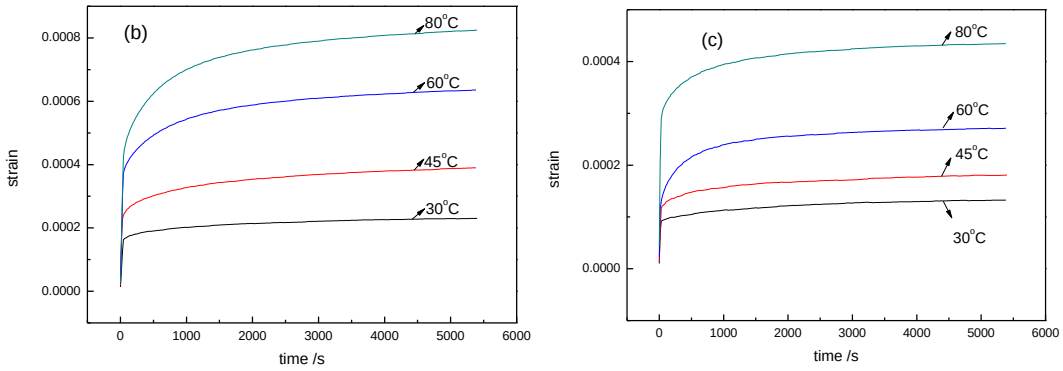

Fig. 6 Three-point bending creep strain curves of TATB-based PBXs at different temperatures under 4 MPa: (a) pure TATB; (b) PBX-1; (c) PBX-2.

3.4 Modeling of the creep behavior

The six-element mechanical model which is regarded as a series connection structure of a Maxwell model and two Kelvin-Voigt models can effectively describe the three-point bending creep behaviors of TATB-based PBXs with high precision.[6] Consequently, the six-element mechanical model is employed to describe the creep process in this study, as shown in Fig. 7. During the creep process, the stress is kept constant, the total strain of polymer composite material PBX could be determined by:

$$\varepsilon(t) = \varepsilon_1 + \varepsilon_2 + \varepsilon_3 + \varepsilon_4 = \frac{\sigma_0}{E_1} + \frac{\sigma_0}{E_2}\left(1 - e^{-t/\tau_2}\right) + \frac{\sigma_0}{E_3}\left(1 - e^{-t/\tau_3}\right) + \frac{\sigma_0}{\eta_4} t \qquad (1)$$

where ε(t) denotes a function of creep strain ε with creep time t, ε_1 is the instantaneous elastic deformation, ε_2 and ε_3 are the high elastic deformation, ε_4 is the viscous flow deformation, σ_0 is the initial stress, E_1 is the elastic modulus of instantaneous elastic deformation, E_2 and E_3 are the elastic modulus of high elastic deformation, τ_2 and τ_3 are the relaxation time, η_4 is the bulk viscosity, respectively.

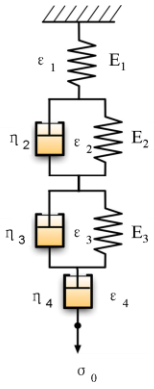

Fig. 7 Schematic drawing of six-element mechanical model.

The experimental curves of creep process at various temperatures are fitted by means of the six-element mechanical model using OriginPro 8.0 software. As an example, Fig. 8 gives the

nonlinear fitting result of PBX-1 at 30 ℃/4 MPa. Experimental result has shown that the six-element mechanical model fits work remarkably well for the experimental data of TATB-based PBXs.

The values of six parameters obtained from the nonlinear fit for PBX-1 and PBX-2 are summarized in Table 3. As can be seen from the fitting results, the parameters including the elastic modulus E_2, E_3 which are associated to the springs of Kelvin-Voigt units, and the bulk viscosity η_4 which is related to the Maxwell dashpot and reflects the irrecoverable creep strain of TATB-based PBXs display a decreasing trend with the temperature. On the other hand, the parameters E_2, E_3, and η_4 seem to increase with the presence of PF2 as polymer binder which indicates an enhanced creep resistance performance. The incorporation of tetrafluoroethylene and hexafluoropropylene monomers in PF2 binder leads to the hindrance of molecular thermodynamic movement. Macroscopically, the rigidity of material increases, leading to an increase of the elastic modulus E_2 and E_3. The relative slide of molecular chain of PF2 binder could be more difficult than that of PF1, resulting in the increase of η_4. The trend of the parameters E_2, E_3, and η_4 with temperate and the molecular structure of polymer binder is consistent with the creep resistance of TATB-based PBXs, revealing that the parameters E_2, E_3, and η_4 may reflect the change of the creep behavior of TATB-based PBXs.

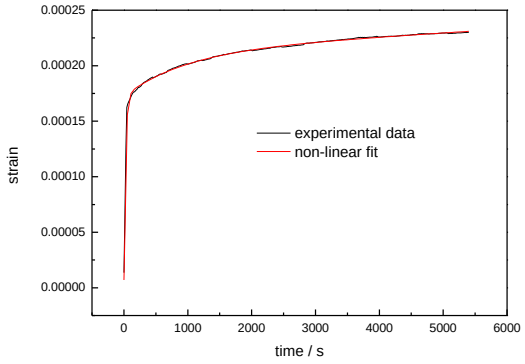

Fig. 8 Three-point bending creep strain curve and non-linear fitting curve of PBX-1 at 30 ℃/4 MPa.

Table 3. The fitting parameters of six-element model under different conditions.

sample	test condition	E_1 /MPa	E_2 /MPa	τ_2 /s	E_3 /MPa	τ_3 /s	η_4 /MPa s	R^2
PBX-1	30 ℃/4MPa	5.760×10^5	9.999×10^4	974.50	2.419×10^4	25.08	1.150×10^9	0.99410
	45 ℃/4MPa	2.720×10^5	4.359×10^4	745.24	1.723×10^4	15.52	4.394×10^8	0.99889
	60 ℃/4MPa	4.431×10^5	2.128×10^4	734.98	1.043×10^4	24.82	3.779×10^8	0.99721
	80 ℃/4MPa	5.341×10^5	1.403×10^4	665.43	8.773×10^3	28.96	2.727×10^8	0.99812
PBX-2	30 ℃/4MPa	4.011×10^5	1.499×10^5	1317.55	4.731×10^4	11.17	2.688×10^9	0.99826
	45 ℃/4MPa	3.148×10^5	1.087×10^5	588.81	3.604×10^4	16.94	9.999×10^8	0.99637
	60 ℃/4MPa	1.655×10^5	3.458×10^4	448.79	3.507×10^4	12.34	8.376×10^8	0.99753
	80 ℃/4MPa	9.403×10^4	4.021×10^4	599.70	1.503×10^4	15.03	7.594×10^8	0.99816

3.5 Creep strain master curve

Fig. 9 depicts the double logarithmic plots of the three-point bending creep strain as a function of creep time for pure TATB and TATB-based PBXs at different temperatures under 4 MPa. As clearly demonstrated in Fig. 9, the pattern of creep strain curves is similar. With increasing temperature, the creep strain gradually reinforces.

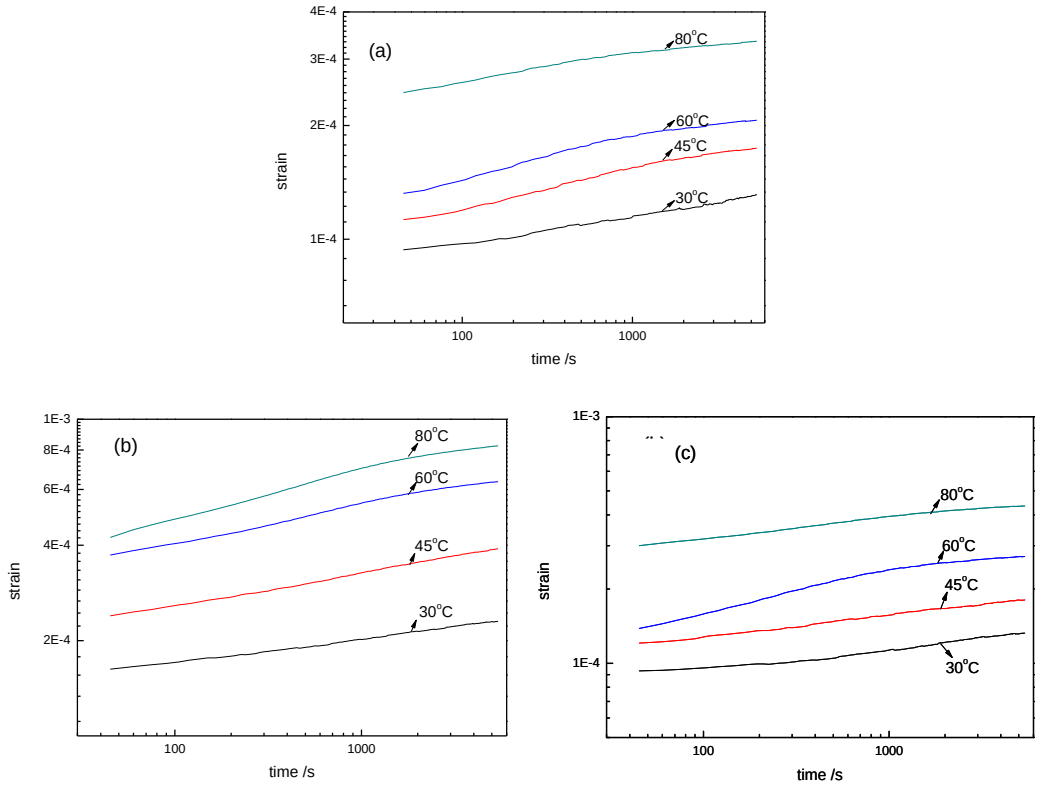

Fig. 9 Double logarithmic plots of three-point bending creep strain for TATB-based PBXs:(a) pure TATB; (b) PBX-1; (c) PBX-2.

The creep behavior could be observed at a high temperature within a short time, also could be observed at a low temperature within a long time. Based on time-temperature superposition principle,[36] the creep strain master curves are obtained at a reference temperature with a left shift of the curves at the temperature higher than the reference temperature and a right shift of the curves at the temperature lower than the reference temperature. The creep strain curve at reference temperature T_r and time t_r is received with a horizontal displacement of the creep strain curve at temperature T and time t:

$$D(T_r, t_r) = D(T_r, t/a_T) = D(T, t) \qquad (2)$$

where a_T is a shift factor. In this work, 30 ℃ is selected as the reference temperature for master curve of creep strain function. Fig. 10 demonstrates the three-point bending creep strain master curves of pure TATB and TATB-based PBXs. With the addition of PF1 as a polymer binder, the predictable creep strain of PBX-1 at 30 ℃/4 MPa is higher than that of pure TATB. Compared with PBX-1, the creep strain master curve of the PBX-2 shifts downward, suggesting that the creep resistance performance is enhanced. The time scale of experimental curves for TATB-based PBXs spans 3 magnitude orders, while the time scale of master curves of TATB-based PBXs spans 7 magnitude orders, indicating that the master curves could simulate the creep behavior of material in a broader time domain. It also can be seen that the creep behavior up to 6.0 years and 15.4 year at 30 ℃ /4 MPa for PBX-1 and PBX-2 could be predicted by the short-term

experimental data (5400 s) acquired at 30 ~ 80 ℃ under 4 MPa, respectively.

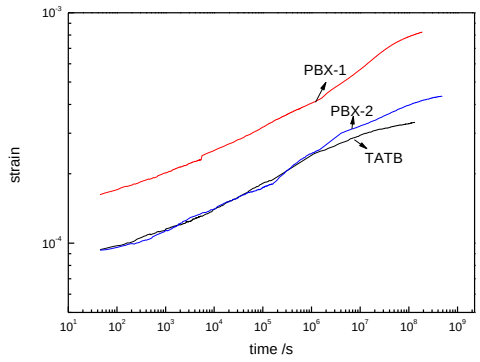

Fig. 10 Three-point bending creep strain master curves of pure TATB and TATB-based PBXs.

4. Conclusions

In this work, the mechanical properties and creep behaviors of the 1,3,5-triamino-2,4,6-trinitrobenzene (TATB)-based polymer bonded explosives (PBXs) containing two kinds of fluoropolymer with different molecular structure as polymer binders at different temperatures and stresses were investigated. The experimental results indicated that: (1) PBX with a copolymer of chlorotrifluoroethylene, vinylidene fluoride, tetrafluoroethylene, and hexafluoropropylene (PF2) showed higher compressive and tensile strength compared to the one with a copolymer of chlorotrifluoroethylene and vinylidene fluoride (PF1) as polymer binder. (2) Similar to static mechanical results, the creep behavior of TATB-based PBXs greatly depended on the molecular structure of fluoropolymer. PBX with PF2 was found to be better creep resistance than the one with PF1 as polymer binder. (3) The six-element mechanical model was successfully used to analyze the non-linear behavior of TATB-based PBXs. The model analysis revealed an increase in the elastic modulus E_2, E_3 and bulk viscosity η_4 for the formulation containing PF2 compared to the one with PF1. (4) Based on time-temperature superposition principle, the creep strain master curves were obtained at a reference temperature of 30 ℃. The creep behavior up to 15.4 year at 30 ℃ /4 MPa could be predicted by the short-term experimental data (5400 s) acquired at 30~80 ℃ under 4 MPa. The experimental results indicated that compared with the formulation with PF1, the creep resistance performance was enhanced by the presence of PF2 with a downward shift of creep strain master curve. The results are helpful for deeper understanding the creep mechanism of TATB-based PBXs and the influence of the molecular structure of polymer binder.

References

1 A. Wuillaume, A. Beaucamp, F. David-Quillot and C. Erad ès, *Propell. Explos. Pyrot.*, 2014, **39**, 390-396.

2 Q. Yan, S. Zeman, and A. Elbeih, *Thermochim. Acta*, 2012, **537**, 1-12.

3 A. Zandiatashbar, C. R. Picu, and N. Koratkar, *Small*, 2012, **8**, 1676-1682.

4 Z. Yao, D. Wu, C. Chen, and M. Zhang, *Compos. Part A: Appl. Sci. Manufac.*, 2013, **50**, 65-72.

5 L. Tang, X. Wang, L. Gong, K. Peng, L. Zhao, Q. Chen, L. Wu, J. Jiang, and G. Lai, *Compos. Sci. Technol.*, 2014, **91**, 63-70.

6 C. Lin, J. Liu, F. Gong, G. Zeng, Z. Huang, L. Pan, J. Zhang and S. Liu, *RSC Adv.*, 2015, **5**, 21376-21383.

7 X. Tu, B. Zhang, X. Wei, and W. Wang, *Chinese J. Energ. Mater.*, 2013, **21**, 306-309.
8 F. J. Gagliardi and B. J. Cunningham. LLNL-CONF-402307, 2008.
9 Z. Liu, H. Xie, K. Li, P. Chen, and F. Huang. *Polym. Test.*, 2009, **28**, 627-635.
10 D. M. Hoffman, *Polym. Eng. Sci.*,, 2003, **43**, 139-156.
11 L. L. Stevens, D. M. Dattelbaum, M. Ahart, and R. J. Hemley, *J. Appl. Phys.*, 2012, **112**, 023523.
12 Q. L. Yan, S. Zeman, and A. Elbeih, *Thermochim. Acta*, 2013, **562**, 56-64.
13 N. K. Bourne and G. T. Gray III, *J. Appl. Phys.*, 2005, **98**, 123503.
14 W. R. Blumenthal, G. T. Gray III, D. J. Idar, M. D. Holmes, P. D. Scott, C. M. Cady and D. D. Cannon, *AIP Conf. Proc.*, 2000, **505**, 671.
15 R. L. Gustavsen, R. J. Gehr, S. M. Bucholtz, R. R. Alcon, and B. D. Bartram, *J. Appl. Phys.*, 2012, **112**, 074909.
16 C. Souers, P. Lewis, M. Hoffman, and B. Cunningham, *Propell. Explos. Pyrot.*, 2011, **36**, 335-340.
17 W. Small IV, E. A. Glascoe, and G. E. Overturf, *Thermochim. Acta*, 2012, **545**, 90-95.
18 P. W. Cooper and S. R.Kurowski, Introduction to the Technology of Explosives, New York: Wiley-VCH, p.21-23, 1996.
19 A. Flores, F. J. Balta Calleja, and T. Asano, *J. Appl. Phys.*, 2001, **90**, 6006-6010.
20 G. Spathis and E. Kontou. *J. Appl. Polym. Sci.*, 2004, **91**, 3519-3527.
21 A. Ranade, K. Nayak, D. Fairbrother, and N. A. D'Souza, *Polymer*, 2005, **46**, 7323-7333.
22. M. Ganß, B. K. Satapathy, M. Thunga, R. Weidisch, P. Pötschke, and A. Janke. *Macromol. Rapid Comm.*, 2007, **28**, 1624-1633.
23. Z. Dai, Y. Gao, L. Liu, P. Pötschke, J. Yang, and Z. Zhang, *Polymer*, 2013, **54**, 3723-3729.
24 Y. Ding, Y. Pan, R. Cai, X. Yu and Y. Yang, *Chinese J. Energ. Mater.*, 2000, **8**, 87-90.
25 C. Lin, S. Liu, X. Tu; Z. Huang, Y. Li, L. Pan, and J. Zhang. *Chinese J. Energ. Mater.*, 2013, **21**: 506-511.
26. National Military Standard of China, Physical Experimental Methods, GJB/772A-97, 1997 (in Chinese).
27. M. Wen, W. Tang, X. Zhou, H. Pang, and F. Zhu, *Chinese J. Energ. Mater.*, 2013, **21**: 490-494.
28 P. Frübing, F. Wang, and M. Wegener, *Appl. Phys. A: Mater. Sci. & Process.*, 2012, **107**, 603-611.
29 Y. P. Khanna and R. Kumar, *Polymer*, 1991, **32**, 2010.
30 H. F. M. Mohamed, E. E. Abdel-Hady, and S. S. Mohamed, *Radiat. Phys. Chem.*, 2007, **76**, 160-164.
31 N. A. Belov, A. A. Zharov, A. V. Shashkin, M. Q. Shaikh, K. Raetzke, and Y. P. Yampolskii. *J. Membrane Sci.*, 2011, **383**, 70-77.
32 J. Claessona and B. Bohloli, *Int. J. Rock Mech. Min. Sci.*, 2002, **39**, 991-1004.
33 Q. Z. Wanga, X. M. Jiaa, S. Q. Koub, Z. X. Zhang, and P.-A. Lindqvist, *Int. J. Rock Mech. Min. Sci.*,2004, **41**, 245-253.
34 H. D. Johnson. MHSMP-78-08, 1978.
35 H. D. Johnson. MHSMP-81-22, 1981.
36 F. Achereiner, K. Engelsing, M. Bastian, and P. Heidemeyer, *Polym. Test.*, 2013, **32**, 447-454.